

Exciton exciton annihilation dynamics in chromophore complexes.

II. Intensity dependent transient absorption of the LH2 antenna system

B. Brüggemann and V. May

Institut für Physik, Humboldt-Universität zu Berlin, Newtonstraße 15, D-12489 Berlin, F. R. Germany

(Received 22 May 2003; accepted 7 November 2003)

Using the multiexciton density matrix theory of excitation energy transfer in chromophore complexes developed in a foregoing paper [J. Chem. Phys. **118**, 746 (2003)], the computation of ultrafast transient absorption spectra is presented. Beside static disorder and standard mechanisms of excitation energy dissipation the theory incorporates exciton exciton annihilation (EEA) processes. To elucidate signatures of EEA in intensity dependent transient absorption data the approach is applied to the B850 ring of the LH2 found in *rhodobacter sphaeroides*. As main indications for two-exciton population and resulting EEA we found (i) a weakening of the dominant single-exciton bleaching structure in the transient absorption, and (ii) an intermediate suppression of long-wavelength and short-wavelength shoulders around the bleaching structure. The suppression is caused by stimulated emission from the two-exciton to the one-exciton state and the return of the shoulders follows from a depletion of two-exciton population according to EEA. The EEA-signature survives as a short-wavelength shoulder in the transient absorption if orientational and energetic disorder are taken into account. Therefore, the observation of the EEA-signatures should be possible when doing frequency resolved transient absorption experiments with a sufficiently strongly varying pump-pulse intensity. © 2004 American Institute of Physics. [DOI: 10.1063/1.1637585]

I. INTRODUCTION

It is of ongoing interest to reveal details of excitation energy transfer dynamics in the various light harvesting antennas of bacteria as well as higher plants. To apply intense laser pulses represents a particular approach although it touches nonphysiological conditions. However, in this way it becomes possible to study higher excited states and new relaxation channels such as exciton exciton annihilation (EEA). Originally, experiments considering EEA have been carried out on dye aggregates (see, for example, Refs. 1 and 2). But there is some recent work where EEA has been demonstrated for different photosynthetic antenna systems. The FMO-complex has been studied in Ref. 3, EEA could be described for the LH1 in Refs. 4, 5, and Refs. 6 and 7 dealt with the LH2.

The standard description of EEA in dye aggregates or light harvesting complexes (LHC) is usually given via a two step process (see, for example, Ref. 8). First, two excitations being in the S_1 -state of the chromophores have to move close together so that their excitation energy can be used to create a higher excited S_n -state ($n > 1$) at one chromophore. This step leaves behind the other chromophore in the S_0 ground-state and is usually named exciton fusion. In a second step an ultrafast internal conversion (IC) process brings back the chromophore which is just in the higher excited S_n -state to the S_1 -state.

It has been explained in detail in the foregoing paper⁹ (Paper I) how to embed this mechanism of EEA into a description based on delocalized (or partially delocalized) exciton states. As a first step in this description one has to introduce higher excited exciton manifolds. Those are positioned on energy scale upon the singly excited electronic

states of the LHC leading to the ordinary exciton. In this way single-exciton states are followed by two exciton states which are formed either by two simply excited chromophores (excited into the S_1 -state) or by a single doubly excited chromophore (put into the S_n -state). In the same way one can also construct higher excited multiexciton (MX) manifolds. Now, EEA appears as a simple nonradiative transition from a higher to a lower exciton manifold. For example, a two-exciton state decays into a state of the single-exciton manifold if its component related to a doubly excited state of a single chromophore is nonzero. This nonzero component opens the decay channel from the two-exciton manifold via an IC process to the single-exciton manifold. If the IC process is assumed to be fast compared to all other processes of exciton motion EEA can be accounted for via particular rates in a respective MX density matrix theory. As a main result of part I we obtained besides correct formulas an approximate version of this rate which is most appropriate for numerical simulations. This rate expression is obtained as a product of an IC rate (identical for all chromophores) and of an overlap expression between the probability to have a double excitation at a certain chromophore and the probability to have a singly excited chromophore.

With this EEA density matrix theory available the present paper discusses simulations of transient absorption spectra. Our computations concentrate on the B850 ring of the LH2 of *rhodobacter sphaeroides* (for a recent overview, see Ref. 10). To account properly for EEA the 18 Bacteriochlorophylls (BChls) which form the B850 ring have to be modeled as three-level systems. Therefore, we introduce beside the Q_y -excitation a higher excited state which should be separated from the first excited Q_y -state by the same ener-

getic distance as the first excited state from the ground state. The delocalized MX states are formed by the electronic interchromophore coupling. In the simulations we included the ground state, the single exciton manifold and the two exciton manifold. Energetic relaxation in the one and the two-exciton manifold is caused by the coupling to the protein environment, whereas the EEA is mainly determined by local vibrations participating in the IC process. Furthermore, as it is well-accepted and has been demonstrated recently by single molecule spectroscopy^{11–16} any LHC is characterized by a certain amount of static disorder, i.e., each complex has a slightly different spectrum caused by a differing microscopic surrounding. This phenomenon will also be considered, and we will compute *frequency dispersed* transient absorption spectra.

Computations on pump–probe spectra for dye aggregates and antenna systems, in particular for the LH2 have been published at different places.^{17–26} However, all these approaches (at least within the numerical calculations) stay on a description which is of third-order in the field-strength. As it is well known (cf., e.g., Ref. 21) such a treatment does not include two-exciton state population but only coherences among the two and the single exciton states. This fact indicates that our approach which describes EEA and thus requires the incorporation of two-exciton (and even higher manifold) populations has to go beyond all these standard theories based on third-order response functions.

The paper is organized as follows: In the next section the central ideas of the MX theory accounting for EEA are quoted briefly. Afterwards, we describe in Sec. III how to compute differential absorption spectra. Section IV discusses results followed by some concluding remarks in Sec. V. Some preliminary results on the description of EEA can be already found in Refs. 27 and 28.

II. MULTIEXCITON DENSITY MATRIX THEORY

Let us start with a short overview on the main ideas of the MX density matrix theory. More details can be found in part I and also in Ref. 25. In a first step we have to define the model used to describe excitation energy dynamics in the ring antenna. There has been a lot of computational work done on the electronic structure of this system (cf. Refs. 29–33) either on an *ab initio* level as well as within a semiempirical approach but, so far, all these studies exclusively concentrate on single exciton states. If one tries to incorporate two exciton states or even higher excitations one has to start from an appropriate constructed model which parameters have to be fixed by a comparison with experimental data.

To get this model we start with the various BChl positioned at the sites $m = 1, \dots, 18$. Every molecule will be characterized by *three* distinct (adiabatic) electronic states φ_{ma} with electronic quantum number a comprising the ground-state quantum number $a = g$, that for the first excited Q_y -state $a = e$, and that for the higher excited state $a = f$. The respective energies are denoted as ϵ_{ma} . Excitation energy transfer between different BChl is caused by the electronic inter-BChl coupling. Due to the presence of the higher excited states φ_{mf} this coupling contains contributions which have been not calculated within semiempirical or *ab initio*

schemes. However, if one takes the approximation of dipole–dipole interaction every coupling can be easily determined (cf. Ref. 25).

All the excitation energies and the electronic couplings are modulated by the variety of vibrational degrees of freedom (DOF) among them localized intra-BChl vibrations as well as delocalized vibrations of the whole protein scaffold. The latter mainly initiate electronic excitation energy dissipation within a given exciton manifold while the first together with nonadiabatic couplings (between φ_{mf} and φ_{me}) are responsible for EEA.

The MX states $|\alpha_N\rangle$ (with quantum number α_N where N indicates the respective manifold) are introduced as the *eigenstates* of the electronic part of the whole Hamiltonian H_{B850} of the B850 ring. They appear as superposition states of locally excited states $|\{me, nf\}_N\rangle$ according to

$$|\alpha_N\rangle = \sum_{\{me, nf\}_N} C_{\alpha_N}(\{me, nf\}_N) |\{me, nf\}_N\rangle. \quad (1)$$

The states $|\{me, nf\}_N\rangle$ refer to a N -fold excitation of the B850 ring, with the BChl at m_1, \dots, m_M in the first excited state and the BChl at n_1, \dots, n_N in the higher state. The numbers M and N are related to N by the condition $N = M + 2N$ when carrying out the summation in Eq. (1). Of course, the notation with an arbitrary N is of less importance here, since the concrete computations are restricted to the incorporation of the two-exciton manifold only.

Besides the definition of the MX states, Eq. (1) results in the coefficients C_{α_N} and also in the MX energies $E(\alpha_N) = \hbar\Omega(\alpha_N)$. These quantities are used to rewrite H_{B850} , first leading to the free MX part, H_{MX} . The coupling to vibrational coordinates described by $H_{\text{vib}}(\alpha_N, \beta_N)$ can be diagonal as well as off-diagonal with respect to the MX-state. Moreover, two main groups of coordinates separately enter $H_{\text{vib}}(\alpha_N, \beta_N)$, belonging to intermolecular (protein) vibrations and intramolecular vibrations. Intermanifold transitions originated by the nonadiabatic coupling between the higher excited and the first excited state of the individual BChl of the ring is accounted for by H_{nonad} . All contributions to H_{B850} have been described in detail in Paper I except the coupling H_{field} to the radiation field which is introduced in the Appendix. In particular, expressions are given there for the MX transition dipole matrix elements $\mathbf{d}(\alpha_{N+1}, \beta_N)$ which calculation is based on the dipole operator $\hat{\mu}_{B850}$ of the complete ring antenna.

To come into contact with data obtained from ultrafast optical experiments one has to calculate the time-dependent expectation value of the dipole operator $\hat{\mu}_{B850}$ (see Sec. III). This expectation value defines the macroscopic polarization (which enters Maxwell's equations) and reads in the present approach as $\langle \hat{\mu}_{B850}(t) \rangle = \text{tr}_{MX} \{ \hat{\mu}_{B850} \hat{\rho}(t) \}$, i.e., the expectation value follows from a trace with respect to the MX states which includes $\hat{\mu}_{B850}$ and the MX (reduced) density operator $\hat{\rho}(t)$. Once the trace has been computed we meet the MX density matrix $\rho(\alpha_M, \beta_N; t) = \langle \alpha_M | \hat{\rho}(t) | \beta_N \rangle$ as the central quantity to be determined. The diagonal elements $\rho(\alpha_M, \alpha_M; t) = P(\alpha_M, t)$ represent the MX level populations, whereas off-diagonal elements define the various coherences. Those can be ordered with respect to intramanifold

coherences indicating the presence of excitonic wave packets in the particular manifold, and intermanifold coherences reflecting optical excitations and thus the presence of transition polarizations in the system.²⁷

In Paper I we focused on details how to derive the MX density matrix equations including EEA. This has been done in the framework of an MX-vibrational representation where $\rho(\alpha_M, \beta_N; t)$ followed from a computation of the trace with respect to all vibrational DOF. As a result of this procedure we obtained a type of density matrix equations which is often named multilevel Redfield equation (cf., for example, Refs. 25, 34). In particular, a version has been taken where any coupling between coherences and populations induced by the dissipative action of the vibrational DOF have been removed (secular approximation and Bloch model). This restriction easily enables us to put back the notation into an operator version of the density matrix equations which is particular useful when considering the coupling to the radiation field. It reads

$$\begin{aligned} \frac{\partial}{\partial t} \hat{\rho}(t) = & -i(\mathcal{L}_{\text{MX}} + \mathcal{L}_{\text{field}}(t))\hat{\rho}(t) \\ & - (\mathcal{R}_{\text{MX-pro}} + \mathcal{R}_{\text{EEA}})\hat{\rho}(t). \end{aligned} \quad (2)$$

The Liouville superoperator \mathcal{L}_{MX} stands for the commutator with the free MX-part of H_{B850} . The commutator with the field-dependent part of H_{B850} is abbreviated by $\mathcal{L}_{\text{field}}$. MX energy relaxation, EEA and dephasing is accounted for by the superoperator $\mathcal{R}_{\text{MX-pro}} + \mathcal{R}_{\text{EEA}}$. As it has been discussed, for example, in Ref. 35 the used type of dissipation introduced into the MX density matrix equations of Paper I can be described by superoperators which are of the so-called Lindblad form. The contributions caused by the coupling to intermolecular (protein) vibrations read

$$\begin{aligned} \mathcal{R}_{\text{MX-pro}}\hat{\rho}(t) = & \sum_N \sum_{\alpha_N, \beta_N} k^{\text{MX-pro}}(\alpha_N \rightarrow \beta_N) \left\{ \frac{1}{2} [|\alpha_N\rangle \right. \\ & \left. \times \langle \alpha_N |, \hat{\rho}(t)]_+ - |\beta_N\rangle \langle \alpha_N | \hat{\rho}(t) | \alpha_N\rangle \langle \beta_N | \right\}. \end{aligned} \quad (3)$$

The intramanifold transition rates $k^{\text{MX-pro}}$ are those given in Eq. (16) of Paper I. They are mainly determined by the MX spectral density \mathcal{J} (cf. Appendix C).

Next we turn to the dissipation superoperator which accounts for the EEA process. Concentrating only on transitions from higher to lower manifolds (the reverse are energetically unfavorable) we have

$$\begin{aligned} \mathcal{R}_{\text{EE}}\hat{\rho}(t) = & \sum_N \sum_{\alpha_N, \beta_{N-1}} k^{\text{EEA}}(\alpha_N \rightarrow \beta_{N-1}) \left\{ \frac{1}{2} [|\alpha_N\rangle \right. \\ & \left. \times \langle \alpha_N |, \hat{\rho}(t)]_+ - |\beta_{N-1}\rangle \langle \alpha_N | \hat{\rho}(t) | \alpha_N\rangle \langle \beta_{N-1} | \right\}. \end{aligned} \quad (4)$$

In Paper I a formula for k^{EEA} has been derived which concentrates on the transition from the two-exciton to the single-exciton manifold. It is of second order in the nonadiabatic coupling between the state φ_f and φ_e and fully accounts for the mutual displacement of the respective potential energy surfaces (PES) U_f and U_e . Of course, both mentioned effects are included into the MX representation.

Although it looks interesting how MX effects alter the IC rate it suffices for the present purposes to take an expression for k^{EEA} , where MX-effects are only considered with respect to the matrix elements of the nonadiabatic coupling. According to Paper I we use

$$k^{\text{EEA}}(\alpha_2 \rightarrow \beta_1) = \sum_m |C_{\beta_1}(me)C_{\alpha_2}(mf)|^2 k_{f \rightarrow e}^{\text{IC}}, \quad (5)$$

where the EEA rate is given by the single chromophore internal conversion rate $k_{f \rightarrow e}^{\text{IC}}$ times the overlap between the probability to have a double excitation at a certain BChl and the probability to have a singly excited BChl. Since the state φ_f is only characterized as the initial state of a very fast IC-process, but otherwise not very precisely known the used approximation for k^{EEA} seems reasonable.

III. TRANSIENT ABSORPTION SPECTRA

It has been explained at different places how to compute femtosecond transient absorption (see, for example, Refs. 17–26, 36). But as shortly discussed in the introductory part our description has to go beyond any theory based at least on a third-order expansion in the field-strength. This main difference to the standard descriptions of pump-probe spectroscopy is originated by the incorporation of EEA. Therefore we choose an approach which avoids perturbation theory in the pump-field.^{25,36}

When discussing a pump probe experiment the applied field contains a pump as well as a probe part (abbreviated in the following by “pu” and “pr,” respectively) and reads

$$\mathbf{E}(\mathbf{r}, t) = \sum_{p=\text{pu,pr}} \mathbf{e}_p E_p(t) e^{i(\mathbf{k}_p \mathbf{r} - \omega_p t)} + \text{c.c.} \quad (6)$$

The unit vectors of the field polarization are denoted by \mathbf{e}_p , $E_p(t)$ are the field amplitudes, and the wave vectors and frequencies are given by \mathbf{k}_p and ω_p , respectively. In the general case the induced polarization may cover any mixture of these partial waves

$$\mathbf{P}(\mathbf{r}, t) = \sum_n \mathbf{e}(n) P^{(n)}(t) e^{i(\mathbf{k}(n)\mathbf{r} - \omega(n)t)}. \quad (7)$$

Here, n comprises the numbers n_{pu} and n_{pr} both extending from $-\infty$ to ∞ , $\mathbf{e}(n)$ denotes the polarization unity vector, and we have set $\mathbf{k}(n) = \sum_p n_p \mathbf{k}_p$ and $\omega(n) = \sum_p n_p \omega_p$ ($p = \text{pu, pr}$).

To get the probe pulse absorption one has to determine the probe pulse induced polarization $P_{\text{pr}}(t)$ which is given by the part of the complete polarization \mathbf{P} propagating into the direction \mathbf{k}_{pr} . Once this has been done the frequency dispersed absorption signal $A_{\text{pr}}(\omega)$ can be deduced from the Fourier transform of $P_{\text{pr}} \exp(-i\omega_{\text{pr}} t)$ and $E_{\text{pr}} \exp(-i\omega_{\text{pr}} t)$ according to (the tilde at the Fourier-transformed fields reminds of the inclusion of the carrier frequency)

$$A_{\text{pr}}(\omega, E_{\text{pu}}) = \frac{4\pi\omega}{c} \text{Im} \frac{\tilde{P}_{\text{pr}}(\omega, E_{\text{pu}})}{\tilde{E}_{\text{pr}}(\omega)}. \quad (8)$$

In defining A_{pr} we indicated the dependence on the pump field. The differential absorption signal simply follows as $\Delta A_{\text{pr}}(\omega, E_{\text{pu}}) = A_{\text{pr}}(\omega, E_{\text{pu}}) - A_{\text{pr}}(\omega, E_{\text{pu}} = 0)$.

There exists different treatments to select the contribution P_{pr} from the overall polarization. If the medium response is described in the framework of a third-order response function a direct selection becomes possible.¹⁸ However, this standard treatment cannot be used in the present case since it does not incorporate EEA. To include the necessary two-exciton populations at least a fifth-order response function theory would become necessary. In such a case it seems more appropriate to directly calculate the polarization without any perturbation expansion with respect to the applied pump and probe pulses. Therefore, we have to start from the following expression for the total polarization

$$\mathbf{P}(\mathbf{r}, t) = \frac{1}{\Delta V(\mathbf{r})} \sum_{\text{LHC} \in \Delta V(\mathbf{r})} \text{tr}_{\text{MX}} \{ \hat{\mu}_{\text{B850}} \hat{\rho}(t) \}. \quad (9)$$

The formula describes a spatial averaging of the polarization contributions of all LHC contained in the volume $\Delta V(\mathbf{r})$ around the spatial point \mathbf{r} where the (macroscopic) polarization should be determined. As already stated the single LHC polarization follows from the MX trace expression defined via the LHC dipole operator and the MX density matrix. Therefore, the polarization and in particular P_{pr} can be determined via a direct computation of the MX density matrix accounting for both field contributions directly in the respective equations of motion [cf. Eq. (2)].

To select P_{pr} from Eq. (9) we follow^{36,37} and propagate the density matrix equations repeatedly by taking the pump field with different constant phase factors $\exp(i\phi)$ [abbreviating the spatial part of the carrier waves appearing in Eqs. (6) and (7)]. This results in a phase dependence $\mathbf{P}(\phi)$ of the overall polarization (note that any other argument has been removed for a moment). If the combination $[\mathbf{P}(0) + \mathbf{P}(\pi/2) + \mathbf{P}(\pi) + \mathbf{P}(3\pi/2)]/4$ is chosen (and the carrier wave as well as the polarization vector \mathbf{e} have been removed) the desired probe field induced polarization P_{pr} is obtained. Of course to meet the requirements of a pump-probe experiment a sufficient weak probe field compared to the pump field has to be used.

If ΔA_{pr} should be determined in dependence on the delay time τ_{del} between the pump and the probe pulse repeated propagations of the whole density matrix equations are necessary. This becomes computational very expensive if static disorder has to be accounted for. Since a direct disorder averaging requires the consideration of many different representatives of the disordered ensemble of LHC we apply an approach where only a single density matrix propagation per ensemble representative is needed. However, it is only valid for such a delay between the pump and the probe pulse where any direct pulse overlapping is already absent.

The reduction to a single density matrix propagations to determine ΔA_{pr} in dependence on τ_{del} becomes possible if we linearize \hat{P}_{pr} in Eq. (8) with respect to the weak probe field, i.e., if we let ΔA_{pr} become independent on the probe field. This treatment is somewhat standard (see, for example, Refs. 19, 25), but here the approach of Ref. 19 is generalized to an inclusion of MX energy dissipation and dephasing as well as to the inclusion of a finite pump-pulse duration.

The basic expression for ΔA_{pr} derived in Appendix B is valid for all exciton manifolds and includes diagonal as well

as off-diagonal MX density matrix elements. For the concrete computations discussed in the following it suffices to restrict up to the two-exciton manifold. Furthermore, to remain sufficient simple here we concentrate on the part $A_{\text{pr}}^{(\text{pop})}$ of the whole expression which exclusively is determined by MX-level populations. (The expression determined by off-diagonal MX density matrix elements can be found in the Appendix.) We get

$$\begin{aligned} \Delta A_{\text{pr}}(\omega, \tau_{\text{del}}) = & \frac{4\pi\omega n_{\text{LHO}}}{\hbar c} \left(\sum_{\beta_1} |d(0, \beta_1)|^2 g(\beta_1, 0; \omega) \right. \\ & \times (P(0; \tau_{\text{del}}, E_{\text{pu}}) - 1 - P(\beta_1; \tau_{\text{del}}, E_{\text{pu}})) \\ & - \sum_{\alpha_1, \beta_2} |d(\alpha_1, \beta_2)|^2 g(\beta_2, \alpha_1; \omega) \\ & \times (P(\alpha_1; \tau_{\text{del}}, E_{\text{pu}}) - P(\beta_2; \tau_{\text{del}}, E_{\text{pu}})) \\ & - \sum_{\alpha_2, \beta_3} |d(\alpha_2, \beta_3)|^2 g(\beta_3, \alpha_2; \omega) \\ & \left. \times P(\alpha_2; \tau_{\text{del}}, E_{\text{pu}}) \right). \quad (10) \end{aligned}$$

For simplicity the disorder averaging has been replaced by a multiplication with the density n_{LHC} of the ring antennae in the probe volume. Furthermore, the labeling “pop” has been removed. The dipole matrix elements follow from those introduced in Appendix A but multiplied with the polarization unity vector of the probe-pulse field. The various g -functions determining the Lorentzian line shape of the different inter-manifold transitions can also be found in Appendix B. The first term on the right-hand side of Eq. (10) covers the ground-state bleaching contribution $[\sim P(0) - 1]$ and the stimulated emission part $\sim P(\beta_1)$, whereas excited-state absorption (from the single-exciton states) is given by the part $\sim P(\alpha_1)$ of the second term. It also contains stimulated emission via transitions from two-exciton states to single-exciton states $[\sim P(\beta_2)]$. Excited state absorption from the two-exciton to the three-exciton states is given by the last term. Because we assume $P(\beta_3) = 0$ this last term does not contain a three-exciton population. But it cannot precisely answered if we are really working in such a pump-intensity regime where $P(\beta_3)$ remains small.

The standard linear absorption into the single-exciton manifold follows if the second and third summation are removed and if in the first one the population difference $P(0; \tau_{\text{del}}, E_{\text{pu}}) - P(\beta_1; \tau_{\text{del}}, E_{\text{pu}})$ is replaced by 1, i.e., the ground-state equilibrium distribution. Therefore, the differential absorption ΔA_{pr} can be deduced from A_{pr} by replacing $P(0; \tau_{\text{del}}, E_{\text{pu}})$ by $P(0; \tau_{\text{del}}, E_{\text{pu}}) - 1$. Equation (10) is a well known formula for calculating transient absorption spectra^{17,19,20,23} and will be confronted in the following with a description where both pulses are considered nonperturbatively.

For further use in the following section we quote the asymptotic form of ΔA_{pr} , i.e., for $\tau_{\text{del}} \rightarrow \infty$ (of course in the present context this means that τ_{del} enters the range of some picoseconds). The asymptotic form reads

$$\begin{aligned} \Delta A_{\text{pr}}(\omega, \infty) &= \frac{4\pi\omega n_{\text{LHC}}}{\hbar c} (1 - P(0; \infty, E_{\text{pu}})) \\ &\times \sum_{\alpha_1} \left(-2|d(\alpha_1, 0)|^2 g(\alpha_1, 0; \omega) \right. \\ &\left. + \sum_{\beta_2} |d(\beta_2, \alpha_1)|^2 g(\beta_2, \alpha_1; \omega) \right) f_{\text{th}}(E(\alpha_1)). \end{aligned} \quad (11)$$

The expression assumes that for $\tau_{\text{del}} \rightarrow \infty$ any population of the two-exciton levels has been disappeared according to EEA. However, a thermal distribution $f_{\text{th}}(E(\alpha_1))$ among the single-exciton states could be formed since any recombination from the single-exciton levels to the ground-state can be neglected at the considered time scale. Note that f_{th} is normalized to 1 and that $1 - P(0) = \sum_{\alpha_1} P(\alpha_1)$. Both relations allow to completely express $\Delta A_{\text{pr}}(\omega, \infty)$ by the pump-field dependent ground-state population $P(0)$. Since $\Delta A_{\text{pr}}(\omega, \infty)$ has a pronounced minimum at 850 nm we take $\Delta A_{\text{pr}}(\lambda = 850 \text{ nm}, \infty)$ to introduce normalized transient abortion spectra

$$\Delta A_{\text{pr}}^{(\text{norm})}(\omega, \tau_{\text{del}}) = \frac{\Delta A_{\text{pr}}(\omega, \tau_{\text{del}})}{\Delta A_{\text{pr}}(\lambda = 850 \text{ nm}, \infty)}. \quad (12)$$

The introduction of such a normalized absorption has the advantage that all curves presented in the following have the same minimum for large delay times irrespective of the applied pump beam intensity. Furthermore, if disorder is neglected for these large delay times the curves completely coincide since the dependence on the ground-state population is canceled. This easily allows to find signatures of EEA in the spectra.

IV. RESULTS AND DISCUSSION

Before presenting the results of our simulations we have to fix all parameters entering the model. As it is well-known the LH2 of *rhodobacter sphaeroides* inhibits a waterwheel-like arrangement of 18 strongly coupled BChls. They are paired to nine dimers and absorbing at 850 nm thus forming the so-called B850 part.^{8,10} Nine additional BChl are positioned in a second concentric ring and absorb at 800 nm (the B800 part). In contrast to the B850 part it is characterized by a weaker inter-BChl coupling.

Since it is not our aim to give a comprehensive description of the LH2 we choose a model which is simple enough but includes EEA and can reproduce the respective part of the measured transient absorption spectra. Therefore, we remove the B800 part, thus neglecting possible relaxations from it to the B850 part and concentrate exclusively on the B850 ring.

For the Q_y -state (in our notation the state with energy ε_e) we use the value equal to 799 nm. As already discussed in various papers (see, e.g., Ref. 25) the concrete assignment of the higher excited state (S_n -state, here with energy denoted by ε_f) is impossible. This uncertainty, of course, is related to the fact that a dense spectrum of electron-vibrational excitations exists in the energetic range of a

doubled Q_y -excitation. If the spectrum is replaced by a single effective level its concrete energetic positions is influenced by the density of states related to the original spectrum. But the introduction of ε_f becomes only important if the related transition dipole moments are large enough to allow for a noticeable strong coupling to delocalized two-exciton states formed by two Q_y -excitation. It has been already confirmed by the early measurements of Ref. 39 that the transition dipole moments are large enough for an efficient coupling. Therefore, we take the dipole-moment of the $S_1 \rightarrow S_n$ transition of BChl of a similar magnitude as d_{eg} , and the latter is set equal to 6.32 D. Furthermore, a blue shift of 100 cm^{-1} is introduced for the $S_1 \rightarrow S_n$ transition energy of each chromophore with regard to the $S_0 \rightarrow S_1$ transition.

The earlier debate about the concrete values of the electronic inter-BChl coupling more or less settled now, here we follow the suggestion of Ref. 10 and take the nearest neighbor coupling as alternating between the two values 322 and 288 cm^{-1} . Because of the close packing of the chromophores these values are beyond a simple dipole-dipole interaction. The next but one neighbored coupling and all other contributions can be described within a dipole-dipole interaction model (cf., e.g., Ref. 29). Respective contributions change the arrangement of the energy levels a little bit. But this is more important in the B800 region and for the B800 to B850 energy transfer, and plays only a minor role for the linear and transient absorption spectra in the B850 region. This justifies a restriction on nearest neighbor coupling when studying the B850 part alone. This approximation is also taken when considering all those couplings where the higher-excited level ε_f is involved. Furthermore we assume that the nearest-neighbor contributions of the coupling processes with the transition $\varphi_e \rightarrow \varphi_f$ at one BChl and the transitions $\varphi_f \rightarrow \varphi_e$ or $\varphi_e \rightarrow \varphi_g$ at another BChl (as well as all reverse processes) are described by the same coupling energy as the basic coupling among the Q_y -excitations.

The depopulation of the higher excited state at a single chromophore which is the last step of the EEA occurs via internal conversion to the first excited state. The IC rate enters the EEA transition rate k^{EEA} , Eq. (5). The respective time constant is taken as $1/k_{f \rightarrow e}^{\text{IC}} = 70$ fs. This value has been determined earlier in Ref. 27 based on the measurements of Ref. 7.

Finally we comment on the used description of the intramanifold transition rates $k^{\text{MX-pro}}$, which are caused by the coupling to the protein vibrations (details can be found in Appendix C). Since nearly nothing is known on details of these vibrations we try to reduce the number of possible additional parameters as much as possible. This is achieved by assuming that any influence is absent of extended (non-local) vibrations of the protein body correlating different BChl. The assumption results in local BChl spectral densities which all should be identical. Furthermore, we restrict the spectral densities on a single type following from the modulation of the Q_y -state. It remains the single chromophore spectral density (which has been adopted to experimental data in Ref. 38)

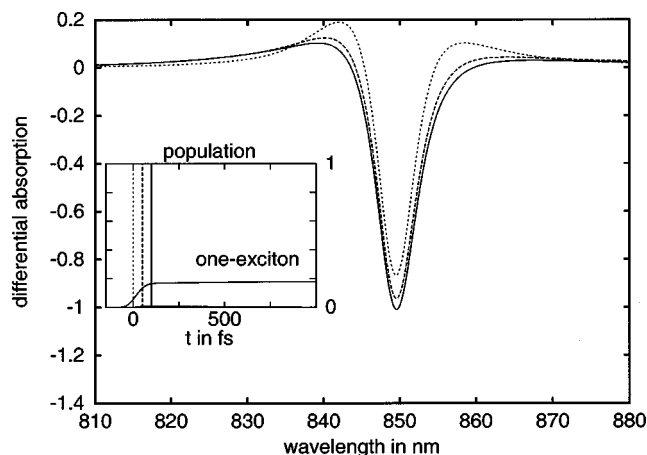


FIG. 1. Normalized frequency resolved transient absorption of the B850 part of the LH2 at different delay times τ_{del} according to Eq. (12) and for the absence of disorder. The pump and the probe pulse are applied at a wavelength of 850 nm and with a duration of 100 fs and 25 fs, respectively. The pump-pulse energy density amounts $8 \mu\text{J}/\text{cm}^2$. Dotted curve: $\tau_{\text{del}}=0$, dashed curve: $\tau_{\text{del}}=50$ fs, full curve: $\tau_{\text{del}}=100$ fs. The inset shows the time evolution of the total population of the one and the two-exciton manifold. Vertical lines mark the delay times at which the transient absorption has been calculated.

$$J_e(\omega) = j_e \sum_{\nu=1}^5 \frac{\omega^2}{2\omega_\nu^3} \exp(-\omega/\omega_\nu). \quad (13)$$

The various frequencies are given by $\omega_1=10.5 \text{ cm}^{-1}$, $\omega_2=25 \text{ cm}^{-1}$, $\omega_3=50 \text{ cm}^{-1}$, $\omega_4=120 \text{ cm}^{-1}$, and $\omega_5=350 \text{ cm}^{-1}$. The overall coupling factor j_e is finally used to achieve a fine-tuning of the computed spectra to the measured ones. Since the IC channel is much faster than the intramanifold relaxation caused by $k^{\text{MX-pro}}$ the coupling of the higher excited MX-states to protein vibrations has been neglected. All computations have been carried out for room temperature conditions.

A. Simulation of transient absorption neglecting disorder

To obtain a clear indication of EEA in the transient absorption spectra we start our calculations in neglecting disorder. Of course these results cannot be compared with the experiment. But to make the spectra look like the measured one (of e.g., Ref. 40), we slightly change our parameters for a moment (for the Q_y -state we take 810 nm and we set $j_e=1.5$). As usual in the experiments we use linearly polarized pump and probe pulses with the magic angle (54.7°) between the polarization directions. Both pulses are applied at a wavelength of 850 nm and have a Gaussian envelope with a duration of 100 fs for the pump-pulse and with a shorter duration of 25 fs for the probe-pulse. The shorter duration has been taken to cover the frequency range of interest when calculating frequency resolved transient absorption.

Figures 1 and 2 display the normalized frequency resolved transient absorption (of the B850 part of the LH2) according to Eqs. (8) and (12) and at different delay times. Therefore, the spectra are calculated by treating the action of the pump and the probe-field beyond a perturbative expansion, and we have set $E_{\text{pu}}=50E_{\text{pr}}$. The time-evolution of the

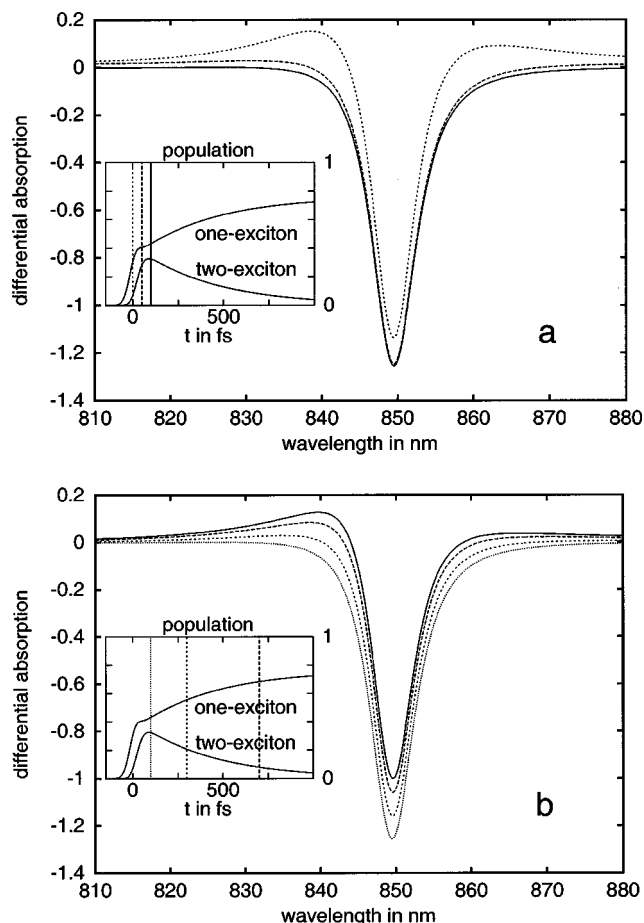


FIG. 2. Normalized frequency resolved transient absorption of the B850 part of the LH2 at different delay times τ_{del} according to Eq. (12) and for the absence of disorder. The pump and the probe pulse are applied at a wavelength of 850 nm and with a duration of 100 fs and 25 fs, respectively. The pump-pulse energy density amounts $64 \mu\text{J}/\text{cm}^2$. (a) Dotted curve: $\tau_{\text{del}}=0$, dashed curve: $\tau_{\text{del}}=50$ fs, full curve: $\tau_{\text{del}}=100$ fs. (b) Dotted curve: $\tau_{\text{del}}=100$, short dashed curve: $\tau_{\text{del}}=300$ fs, dashed curve: $\tau_{\text{del}}=700$ fs, full curve: $\tau_{\text{del}}=1500$ fs. The insets show the time evolution of the total population of the one and the two-exciton manifold. Vertical lines mark the delay times at which the transient absorption has been calculated.

total one-exciton and two-exciton population is shown in the insets of Figs. 1 and 2. Since the spectra of Fig. 1 have been computed for a eight times weaker pump-pulse intensity leading to a negligible two-exciton population, they have to be considered as reference spectra unaffected by EEA.

At 850 nm the transient absorption of Fig. 1 shows a pronounced bleaching. The sharp structure is caused by the fact that in the absence of disorder only the two degenerated states of the one-exciton manifold often denoted as $k \pm 1$ are optically allowed from the ground-state. A clear indication that two-exciton levels are involved is given by the shoulder of $\Delta A_{\text{pr}}^{(\text{norm})}$ around 840 nm. The transient absorption becomes stationary after $\tau_{\text{delay}}=700$ fs what is also obvious by the time-evolution of the one-exciton population. (Of course, the relaxed single-exciton distribution is removed by other processes not involved in our description.)

The behavior is different if the pump-pulse intensity is increased (Fig. 2). First let us take a look at the MX-dynamics shown by the insets of Fig. 2. Here, the strong pumping induces a two-exciton population comparable to the

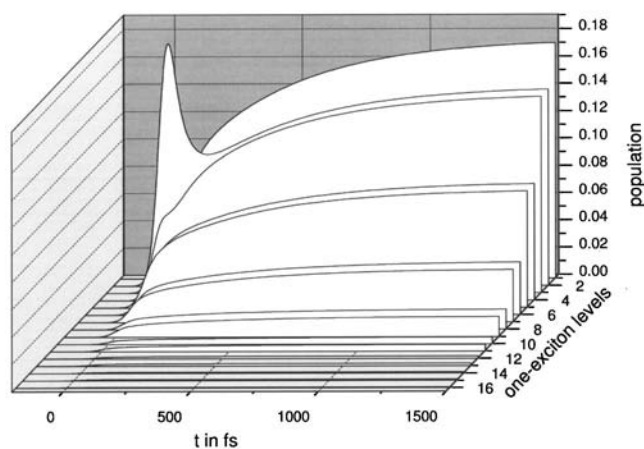


FIG. 3. One-exciton populations of the B850 part of the LH2 vs time after a pump-pulse action at 850 nm, with a duration of 100 fs and with an energy density of $64 \mu\text{J}/\text{cm}^2$.

one-exciton population. And according to EEA there is a rise of the latter population at the expense of the two-exciton population. The notable population of the two-exciton levels up to about 500 fs changes the transient absorption strongly when compared with the case drawn in Fig. 1. At later times,

however, $\Delta A_{\text{pr}}^{(\text{norm})}$ matches the (quasi-) stationary curve of Fig. 1 [because of drawing spectra normalized according to Eq. (12)]. The intermediate change of the transient absorption by two-exciton populations results in a weakening of the bleaching at the main minimum at 850 nm and in the absence of the two shoulders around the minimum. Between 50 fs and 500 fs, $\Delta A_{\text{pr}}^{(\text{norm})}$ remains very small outside the minimum. Only if EEA has removed the two-exciton populations these positive structure reappear. We consider this intermediate behavior as a strong indication for notable two-exciton populations and the action of EEA. As a completion to the discussion led so far Fig. 3 displays the single-exciton population subdivided with respect to the different energies. First, one of the two dipole-allowed states becomes populated by the pump-pulse (the selective population between the two levels results from the linear polarization of the pulse). However, simultaneously a fast redistribution takes place ending up with a thermal population of all levels.

Further insight into the time-evolution of the transient absorption given in Fig. 2 is achieved when separating it into the different contributions contained in Eq. (10). Since the mentioned formula is only valid for a nonoverlapping pump and probe pulse, Fig. 4, starts at a delay-time of 100 fs (part a). Furthermore we note that a complete reproduction of the

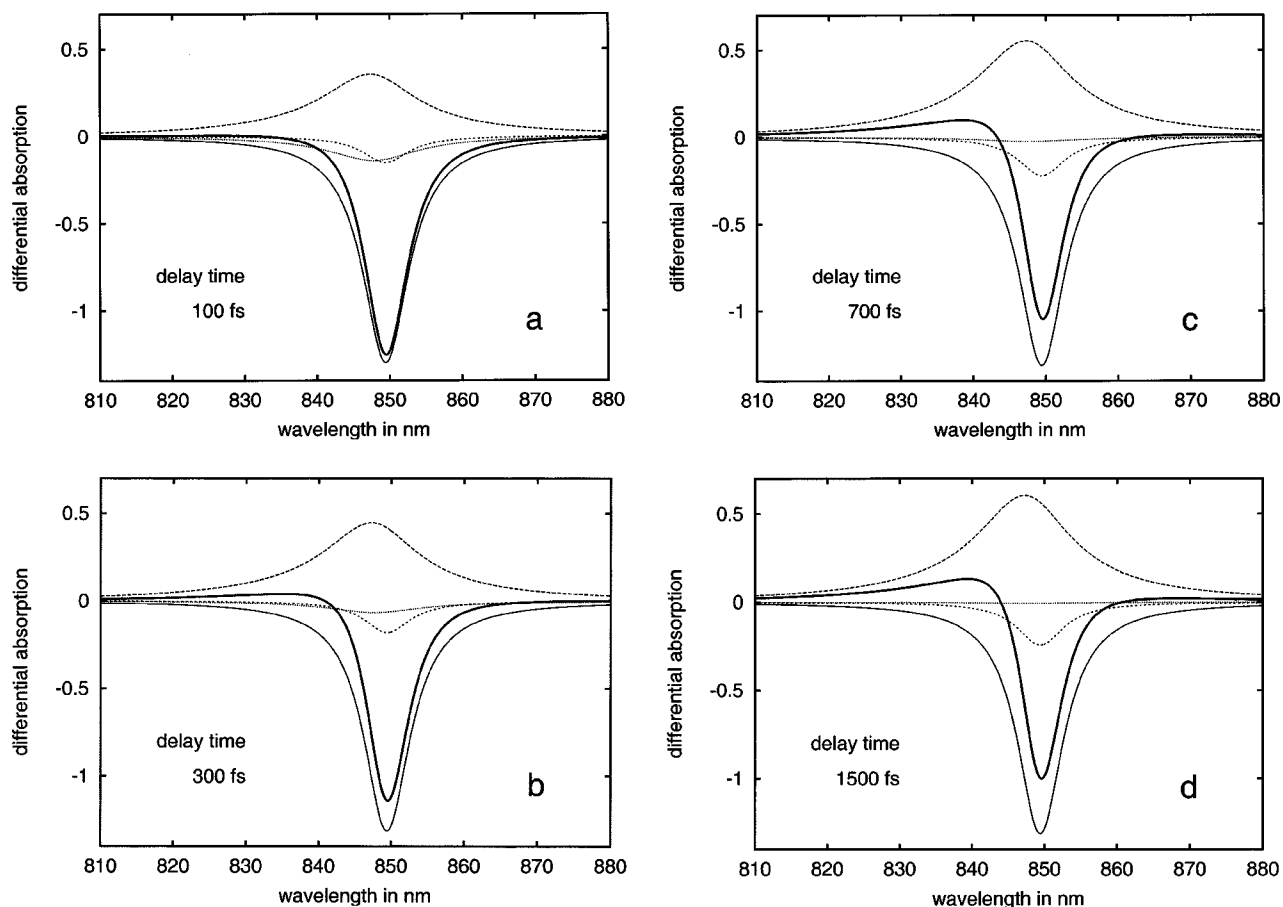


FIG. 4. Separation of the normalized frequency resolved transient absorption of the B850 part of the LH2 into different contributions according to Eqs. (10) and (12) (absence of disorder). The pump and the probe pulse are applied at a wavelength of 850 nm. The pump pulse duration amounts to 100 fs and the energy density $64 \mu\text{J}/\text{cm}^2$. Thick full curve: complete transient absorption, thin full curve: ground-state bleaching, short dashed curve: stimulated emission (from the one-exciton manifold), dashed curve: excited state absorption (from the one-exciton manifold), dotted curve: stimulated emission (from the two-exciton manifold). (a) $\tau_{\text{del}} = 100$ fs, (b) $\tau_{\text{del}} = 300$ fs, (c) $\tau_{\text{del}} = 700$ fs, (d) $\tau_{\text{del}} = 1500$ fs.

results of Fig. 2 is impossible because Eq. (10) assumes an impulsive action of the probe-pulse. Besides the total value of $\Delta A_{pr}^{(norm)}$, Fig. 4 displays the ground-state bleaching, the excited state absorption from the one-exciton into the two-exciton manifold, and stimulated emission from the two-exciton state to the one-exciton state, as well as from the one-exciton state to the ground-state. Comparing all curves for the four chosen delay times (100, 300, 700, and 1500 fs) we first notice the stationary behavior of the ground-state bleaching. This is due to the fact that after the action of the pump-pulse the ground-state depletion has been finished (within our approach) and population redistribution only appears between the one- and the two-exciton manifold. Because of a decreasing two-exciton population the contribution of the stimulated emission from the two to the one-exciton states to $\Delta A_{pr}^{(norm)}$ disappears relatively fast. But this process together with the stimulated emission from the one-exciton to the ground state is responsible for a decrease of the shoulders of the total transient absorption around 850 nm in the delay-time interval up to about 500 fs. For later times $\Delta A_{pr}^{(norm)}$ is only dominated by the excited-state absorption (from the one-exciton to the two-exciton manifold) and, of course, by the ground-state bleaching.

B. Influence of disorder

In order to simulate experimental spectra one has to consider the random orientation of the LH2 in the probe and the fact that structural and energetic disorder is present. Random orientation is taken into account by, first, rotating each ring antenna with randomly chosen Euler angles. Note that the rotation with three different axes has to be used here, caused by the three-dimensional structure of the LH2 and the use of linear polarized laser pulses (cf. Ref. 18). Energetic disorder is considered by randomly distributed Q_y -energies according to a Gaussian distribution with variance $\sigma = 275 \text{ cm}^{-1}$. The disorder leads to a redshift of the absorption spectrum what is compensated by using a higher mean excitation energy of the BChls at 799 nm. To fit the experimental data the overall vibronic coupling factor has been set to $j_e = 0.5$. The averaged spectra have been obtained from Eq. (10) but with n_{LHC} replaced by a summation over 10^4 different LH2 (divided by the respective volume). Of course, the MX-populations of Eq. (10) have been calculated separately for a given disorder configuration [remember that use of Eq. (8) would be too time-consuming].

In Fig. 5 the pump pulse is placed at 847 nm, i.e., slightly to the blue of the main absorption line. It undergoes only a small spectral shift. But due to two-exciton populations and EEA the shoulder at the short-wavelength side of the main absorption clearly observable at $\tau_{del} = 1.5 \text{ ps}$ is suppressed at intermediate times. As discussed in the previous section the suppression of the shoulder and its return at later times as well as the weakening of the bleaching structure is a clear indication for a notable two-exciton population and resulting EEA. Since random spatial orientation has been considered a smaller total (ensemble averaged) population of the one- and two-exciton manifold as in the case of the ordered LH2 (cf. Fig. 2) may lead to a similar extend of changes in

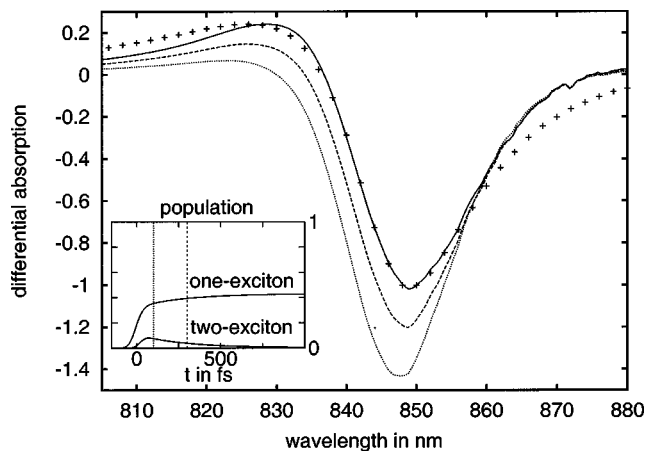


FIG. 5. Normalized frequency resolved transient absorption of the B850 part of the LH2 according to Eqs. (10) as well as Eq. (12) and at different delay times τ_{del} . The pump-pulse acts at 847 nm, with a duration of 100 fs and with an energy density of $64 \mu\text{J}/\text{cm}^2$. Diagonal disorder of 275 cm^{-1} and orientational averaging have been accounted for by sampling over 10^4 configurations. Experimental data (shown by crosses) are taken from Ref. 40 (for a 150 fs long pump pulse with energy density of $100 \mu\text{J}/\text{cm}^2$ and at $\tau_{del} = 1.1 \text{ ps}$). Dotted curve: $\tau_{del} = 100$; dashed curve: $\tau_{del} = 300 \text{ fs}$; full curve: $\tau_{del} = 1.1 \text{ ps}$. The inset shows the time evolution of the population of the one and two-exciton manifolds.

the spectra. The present computations shows that the mentioned signature for EEA indeed survives disorder averaging and should be observable in the experiment.

To further underline the importance of our calculations we compared our simulation with the experimental data of Ref. 40 for the delay of 1.1 ps. In Ref. 40 a 150 fs pulse with a slightly higher energy density has been used, which should give a higher EEA signal, but this would be without any consequence for the considered large delay-time. Our simulations fit the experimental result quite well. The deviation at the red side of the transient absorption could be reduced by either choosing a bigger value of static disorder, introducing intercomplex disorder or an elliptic deformation. Other effects like exciton selftrapping (polaron formation) could also play a role.^{41,42} However, as stated above, this would be beyond the task of the present paper. A somewhat different comparison of the computations accounting for disorder with the experimental data of Ref. 27 is given in Fig. 6. This figure indicates (except for the pump-probe-pulse overlap) that the present approach may reproduce the whole time-evolution of the transient absorption at a particular frequency.

Using a pump pulse with the wavelength 822 nm and the same intensity as before (Fig. 5), the absorption as displayed in Fig. 7 is about four times lesser than in Fig. 5. Therefore the effect of EEA is weaker (note again that the drawn total populations of the one- and two-exciton manifolds underestimate the possible changes in the spectra). Accordingly the weakening of the bleaching structure and only the rise of the lower wavelength shoulder with increasing delay-time can be observed. Furthermore there is a fast redshift of the bleaching maximum, which is caused by intramanifold relaxation. This calculated redshift agrees very nicely with recent experimental data for the LH1 complexes,²⁶ which has a similar but bigger water wheel like the BChl structure called

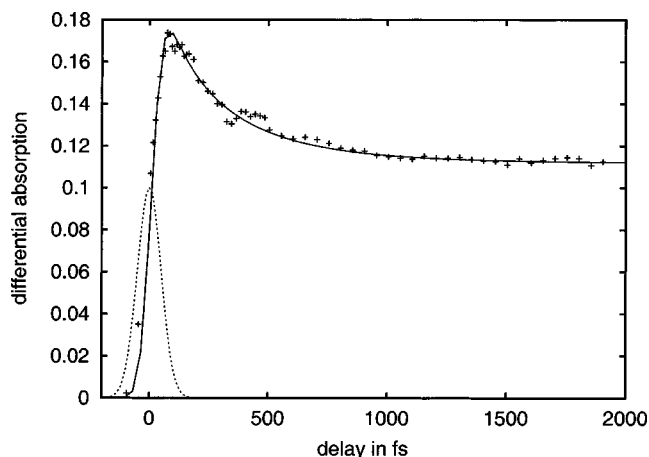


FIG. 6. Non-normalized transient absorption at 847 nm [according to Eqs. (10)] vs time after pump-pulse action and the account for disorder like in Fig. 6. Experimental data (shown by crosses) are taken from Ref. 27. The dotted line displays the envelope of the pump-pulse.

B875. It should be pointed out that, caused by the symmetry of the LH2 system, this spectral shift can only occur if the system inhibits a considerably amount of static disorder.

V. CONCLUSIONS

Our study of exciton exciton annihilation (EEA) processes started in Paper I has been continued to the calculation of quantities observable in the experiment. Special emphasis put on the transient absorption measured in an optical pump-probe experiment. The need to incorporated two-exciton populations does not allow to apply standard-theories based on third-order response functions. Instead, an approach has been taken which accounts for all orders in the pump- and the probe field strength. To understand the time-evolution of the transient absorption in detail an approximate formula was derived separating the whole spectrum into a ground-state bleaching part, into stimulated emission parts (from the two-exciton to the single-exciton manifold as well as from the single-exciton manifold to the ground-state), and into an excited state absorption part (from the one-exciton to the two-exciton manifold).

In order to elucidate signatures of two-exciton populations and EEA in intensity dependent transient absorption data the approach is applied to the B850 ring of the LH2 found in *rhodobacter sphaeroides*. As a main indication the weakening of the single-exciton bleaching structure was found together with an intermediate suppression of long-wavelength and short-wavelength shoulders of the transient absorption around the bleaching structure. The suppression is caused by stimulated emission from the two-exciton to the one-exciton state and the return of the shoulders follows from a depletion of two-exciton population according to EEA. This signature for two-exciton population and resulting EEA survives as a short-wavelength shoulder in the transient absorption if orientational and energetic disorder are taken into account thus indicating the possible observation of this EEA signature when doing frequency resolved transient absorption experiments with sufficiently strongly varying pump-pulse intensity.

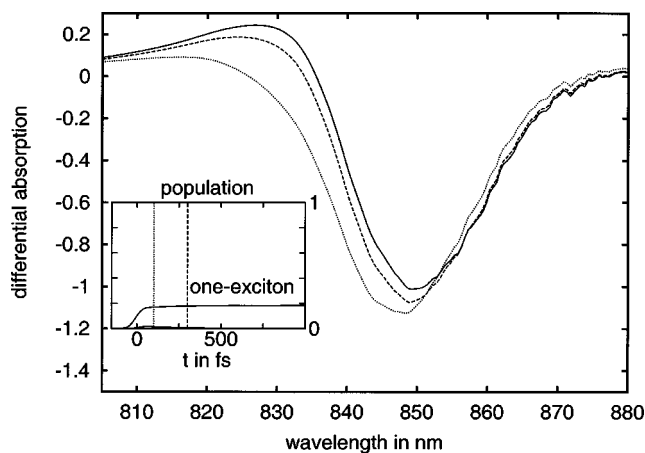


FIG. 7. Normalized frequency resolved transient absorption of the B850 part of the LH2 according to Eqs. (10) as well as Eq. (12) and at different delay times τ_{del} . The pump-pulse acts at 822 nm, with a duration of 100 fs and with an energy density of $64 \mu\text{J}/\text{cm}^2$. Diagonal disorder of 275 cm^{-1} and orientational averaging have been accounted for by sampling over 10^4 configurations. Dotted curve: $\tau_{del}=100 \text{ fs}$, dashed curve: $\tau_{del}=300 \text{ fs}$, full curve: $\tau_{del}=1.1 \text{ ps}$. The inset shows the time evolution of the of population of the one- and two-exciton manifolds.

Of course the obtained results are not restricted to the B850 ring of the LH2. They may be also used for experiments at other biological as well as artificial chromophore complexes to reveal the diversity of relaxation channels at higher optical excitation densities.

ACKNOWLEDGMENTS

We thank Professor Arvi Freiberg for providing us with the experimental data of Fig. 4. The financial support by the Deutsche Forschungsgemeinschaft through Sonderforschungsbereich 450 is gratefully acknowledged.

APPENDIX A: COUPLING TO THE RADIATION FIELD

The coupling to the radiation field is written in the standard form $H_{field} = -\mathbf{E}(t) \hat{\mu}_{B850}$ with the electric field strength $\mathbf{E}(t)$ and the dipole operator $\hat{\mu}_{B850}$ of the complete ring antenna. For any chromophore a dipole-allowed transition from the chromophore ground-state to the first excited state is assumed. Furthermore, a transition from this excited state to the higher excited state becomes also possible, thus allowing for intramolecular excited state absorption. The respective LHC dipole operator can be written

$$\begin{aligned} \hat{\mu}_{B850} &= \sum_m (\mathbf{d}_{eg}^{(m)} |\varphi_{me}\rangle \langle \varphi_{mg}| + \mathbf{d}_{fe}^{(m)} |\varphi_{mf}\rangle \langle \varphi_{me}|) + \text{h.c.} \\ &\equiv \sum_N \sum_{\alpha_{N+1}, \beta_N} \mathbf{d}(\alpha_{N+1}, \beta_N) |\alpha_{N+1}\rangle \langle \beta_N| + \text{h.c.} \end{aligned} \quad (\text{A1})$$

The MX dipole matrix elements given in the second part of this expression can be computed in a similar manner as it has been already done in Paper I for the nonadiabtic coupling. The transition matrix elements from the ground-state into the single-exciton manifold simply follow as

$$\mathbf{d}(\alpha_1, 0) = \sum_k \mathbf{d}_{eg}^{(k)} C_{\alpha_1}^*(ke), \quad (\text{A2})$$

and for the transition from the single-exciton to the two-exciton manifold we get

$$\mathbf{d}(\alpha_2, \beta_1) = \sum_k \sum_{m \neq k} \mathbf{d}_{eg}^{(k)} C_{\alpha_2}^*(me, ke) C_{\beta_1}(me) + \sum_n \mathbf{d}_{fe}^{(n)} C_{\alpha_2}^*(nf) C_{\beta_1}(ne). \quad (\text{A3})$$

APPENDIX B: LINEARIZATION WITH RESPECT TO THE PROBE FIELD

To linearize \tilde{P}_{pr} of Eq. (8) with respect to the weak probe field and, in this way to let become ΔA_{pr} independent on the probe field we start with the complete time-dependence of the MX density operator including all fields $\hat{\rho}(t; \mathbf{E}) = \mathcal{U}(t, t_0; \mathbf{E}) \hat{\rho}(t_0)$. The time evolution superoperator has been denoted by \mathcal{U} and follows via the solution of Eq. (2). To carry out the linearization we separate the total electric field-strength into the pump field $\mathbf{E}_{\text{pu}}(t)$ as well as into the probe field $\mathbf{E}_{\text{pr}}(t)$, and introduce the Liouvillian $\mathcal{L}_{\text{pr}}(t)$ which exclusively describes the interaction with the probe field. Next, the expression for $\hat{\rho}(t)$ will be linearized with respect to the probe field (note that the field dependence will be indicated in the following by denoting the dependence on the pulse envelopes E_{pu} and E_{pr}). Accordingly, the envelope P_{pr} of the polarization induced by the probe field reads

$$P_{\text{pr}}(\mathbf{r}, t) = \frac{i}{\hbar \Delta V(\mathbf{r})} \sum_{\text{LHC} \in \Delta V(\mathbf{r})} \int_{t_0}^t d\bar{t} e^{i\omega_{\text{pr}}(t-\bar{t})} \times \text{tr}_{\text{MX}}\{(\mathbf{e}_{\text{pr}} \hat{\mu}_{\text{B850}}) \mathcal{U}(t, \bar{t}; E_{\text{pu}}) \times [(\mathbf{e}_{\text{pr}} \hat{\mu}_{\text{B850}}), \hat{\rho}(\bar{t}; E_{\text{pu}})]_-\} \times E_{\text{pr}}(\mathbf{r}, \bar{t}). \quad (\text{B1})$$

Here, $\rho(t; E_{\text{pu}})$ denotes the density operator which has been propagated at the presence of the pump field only. Equation (B1) simplifies considerable if the pump and the probe pulse do not overlap and if the duration of the probe pulse is short

compared to any characteristic time of the MX-dynamics. The latter property allows to replace the probe field envelope under the time integral by $E_{\text{pr}}(\bar{t}) \approx \delta(\bar{t} - t_{\text{pr}}) \tau_{\text{pr}} \bar{E}_{\text{pr}}$, i.e., by a δ -function localized at time t_{pr} . The time τ_{pr} determines the finite duration of the pulse around t_{pr} with the mean pulse envelope \bar{E}_{pr} . The respective polarization envelope follows from Eq. (B1) as

$$P_{\text{pr}}(t) = \frac{i\Theta(t-t_{\text{pr}})}{\hbar \Delta V(\mathbf{r})} \sum_{\text{LHC} \in \Delta V(\mathbf{r})} e^{i\omega_{\text{pr}}(t-t_{\text{pr}})} \tau_{\text{pr}} \bar{E}_{\text{pr}} \times \text{tr}_{\text{MX}}\{(\mathbf{e}_{\text{pr}} \hat{\mu}_{\text{B850}}) \mathcal{U}(t-t_{\text{pr}}) \times [(\mathbf{e}_{\text{pr}} \hat{\mu}_{\text{B850}}), \hat{\rho}(\tau_{\text{del}}; E_{\text{pu}})]_-\}. \quad (\text{B2})$$

Note that the time-evolution superoperator describes a field-free evolution since for $t > t_{\text{pr}}$ the pump field is definitely absent. In contrast, the density operator $\hat{\rho}(\tau_{\text{del}}; E_{\text{pu}})$ characterizes the full evolution of the MX-system induced by the interaction with the pump-pulse. Since it is of interest to draw the probe-pulse absorption versus the delay-time $\tau_{\text{del}} = t_{\text{pr}} - t_{\text{pu}}$ (here, t_{pu} is the time at which the pump-pulse reaches its maximum), the MX-density operator has been indicated by τ_{del} instead of t_{pr} .

To carry out the Fourier transformation necessary to get the differential absorption Eq. (8) we have to compute the time-dependence induced by $\mathcal{U}(t-t_{\text{pr}})$. To do this, first we note that in the present type of density matrix equations diagonal and off-diagonal elements are decoupled. Moreover, the restriction to resonance contributions [we only take terms of the trace which oscillate like $\exp(-i\Omega t)$ (with $\Omega > 0$)] is done, and we neglect off-diagonal density matrix elements of the type $\rho(\alpha_{M \pm 2}, \beta_M)$ (they connect non-neighboring exciton manifolds and show a highly oscillatory behavior). If we computed the trace expression in Eq. (B2) the Fourier transformation necessary to get the transient absorption signal Eq. (8) can be carried out. We obtain from Eq. (8) [note $d(\alpha_N, \beta_{N-1}) = \mathbf{d}(\alpha_N, \beta_{N-1}) \mathbf{e}_{\text{pr}}$],

$$A_{\text{pr}}(\omega) = \frac{4\pi\omega}{\hbar c \Delta V(\mathbf{r})} \sum_{\text{LHC} \in \Delta V(\mathbf{r})} \sum_M \sum_{\alpha_M \beta_{M+1}} \text{Im} \left(\sum_{\gamma_M} \frac{d(\alpha_M, \beta_{M+1}) d(\beta_{M+1}, \gamma_M)}{\omega - \tilde{\Omega}(\beta_{M+1}, \alpha_M)} \rho(\gamma_M, \alpha_M; \tau_{\text{del}}, E_{\text{pu}}) - \sum_{\gamma_{M+1}} \frac{d(\gamma_{M+1}, \alpha_M) d(\alpha_M, \beta_{M+1})}{\omega - \tilde{\Omega}(\beta_{M+1}, \alpha_M)} \rho(\beta_{M+1}, \gamma_{M+1}; \tau_{\text{del}}, E_{\text{pu}}) \right). \quad (\text{B3})$$

Here we used $\tilde{\Omega}(\beta_{M+1}, \alpha_M) = \Omega(\beta_{M+1}) - \Omega(\alpha_M) - i\Gamma(\beta_{M+1}) - i\Gamma(\alpha_M)$ with the dephasing rates

$$\Gamma(\alpha_M) = \sum_{\gamma_M} k^{\text{MX-pro}}(\alpha_M \rightarrow \gamma_M)/2 + \sum_{\gamma_{M-1}} k^{\text{EEA}}(\alpha_M \rightarrow \gamma_{M-1})/2$$

[$\Gamma(\beta_{M+1})$ is defined in the same way]. According to the presence of diagonal and off-diagonal MX density matrix elements, i.e., $\rho(\gamma_M, \alpha_M) = \delta_{\gamma_M, \alpha_M} P(\gamma_M) + (1 - \delta_{\gamma_M, \alpha_M}) \Delta \rho(\gamma_M, \alpha_M)$ the absorption A_{pr} can be separated into a term $A_{\text{pr}}^{(\text{pop})}$ governed by the populations $P(\gamma_M)$ and a term $A_{\text{pr}}^{(\text{coh})}$ governed by the (intramanifold) coherences $\Delta \rho(\gamma_M, \alpha_M)$. The latter describes intramanifold dephasing and vanishes on the respective time scale. In contrast $A_{\text{pr}}^{(\text{pop})}$ covers the relaxation of the MX-distribution to an equilibrium distribution of the single-exciton manifold (higher manifolds are depopulated because of the presence of EEA processes). We obtain for the absorption signal determined by the MX-population,

$$A_{\text{pr}}^{(\text{pop})} = \frac{4\pi\omega}{\hbar c \Delta V(\mathbf{r})} \sum_{\text{LHC} \in \Delta V(\mathbf{r})} \sum_M \sum_{\alpha_M \beta_{M+1}} |d(\alpha_M, \beta_{M+1})|^2 g(\beta_{M+1}, \alpha_M; \omega) (P(\alpha_M; \tau_{\text{del}}, E_{\text{pu}}) - P(\beta_{M+1}; \tau_{\text{del}}, E_{\text{pu}})). \quad (\text{B4})$$

Here we introduced the Lorentzian line-shape function,

$$g(\alpha_M, \beta_N; \omega) = \text{Im} \frac{1}{\omega - \tilde{\Omega}(\omega_M, \beta_N)} \\ \equiv \frac{\Gamma(\alpha_M) + \Gamma(\beta_N)}{(\omega - \Omega(\alpha_M, \beta_N))^2 + (\Gamma(\alpha_M) + \Gamma(\beta_N))^2}. \quad (\text{B5})$$

The quantity $A_{\text{pr}}^{(\text{coh})}$ follows from A_{pr} given in Eq. (B3) by replacing ρ by $(1 - \delta)\Delta\rho$. It is responsible for oscillatory structures in the transient absorption which, at least, are caused by a coherent excitation of two levels of the same manifold. It is easy to reduce $A_{\text{pr}}^{(\text{pop})}$ to an expression which only accounts for the first and the second exciton-manifold. The respective expression is given in the main part.

APPENDIX C: PROTEIN SPECTRAL DENSITIES

To get the MX relaxation rates $k^{(\text{MX-pro})}(\alpha_N \rightarrow \beta_N)$ we need certain expressions for the spectral densities $\mathcal{J}(\alpha_N \beta_N, \beta_N \alpha_N; \omega)$. For their derivation we may follow the procedure given in Ref. 25 but generalized here to a three-level model for every BChl. Based on the assumption of a linear coupling of the protein vibrations to the MX states, the $\mathcal{J}(\alpha_N \beta_N, \beta_N \alpha_N; \omega)$ are determined by the square of respective coupling coefficients. Those are the MX representation of the local coupling coefficients describing the coupling of all three BChl electronic levels to the low-frequency vibrations. Consequently, \mathcal{J} can be reduced to expressions with the two-site spectral densities $J(ma, nb; \omega)$ ($a, b = e, f$). Since nothing is known about the MX-protein coupling in the LH2 additional assumptions are necessary to further proceed. In Ref. 25 we suggested how to treat the nonlocal character of $J(me, ne; \omega)$. For the computations in the present paper, however, we take a somewhat different assumption providing sufficiently localized protein vibrations. Then, off-diagonal contributions of $J(ma, nb; \omega)$ can be neglected, and it seems to be a rather good approximation to let become the single-site spectral densities independent on the local BChl. Furthermore, since an efficient IC-process from the S_n state to the Q_y -state is present only a vibrational modulation of the Q_y -state will be considered.

Having all these simplifications in mind the single-exciton spectral density and the two-exciton one, both entering the relaxation rate are obtained as

$$\mathcal{J}(\alpha_1 \beta_1, \beta_1 \alpha_1; \omega) = \sum_m |C_{\alpha_1}(me) C_{\beta_1}(me)|^2 J_e(\omega), \quad (\text{C1})$$

and as

$$\mathcal{J}(\alpha_N \beta_N, \beta_N \alpha_N; \omega) = 4 \sum_{k, m, n} C_{\alpha_2}^*(ke, me) C_{\beta_2}(ke, me) \\ \times C_{\beta_2}^*(ke, ne) C_{\alpha_2}(ke, ne) J_e(\omega), \quad (\text{C2})$$

where $J_e(\omega)$ is the uniform single-site spectral density.

- ¹ V. Sundström, T. Gillbro, R. A. Gadonas, and A. Piskarskas, *J. Chem. Phys.* **89**, 2754 (1988).
- ² H. Stiel, S. Daehne, and K. Teuchner, *J. Lumin.* **39**, 351 (1988).
- ³ V. Gulbinas, L. Valkunas, D. Kuciauskas, E. Katilius, V. Liuolia, W. Zhou, and R. E. Blankenship, *J. Phys. Chem.* **100**, 17950 (1996).
- ⁴ S. E. Bradforth, R. Jimenez, F. van Mourik, R. van Grondelle, and G. R. Fleming, *J. Phys. Chem.* **99**, 16179 (1995).
- ⁵ L. Valkunas, E. Akesson, T. Pullerits, and V. Sundström, *Biophys. J.* **70**, 2373 (1996).
- ⁶ Y.-Z. Ma, R. J. Cogdell, and T. Gillbro, *J. Phys. Chem. B* **101**, 1087 (1997).
- ⁷ G. Trinkunas, J. L. Herek, T. Polívka, V. Sundström, and T. Pullerits, *Phys. Rev. Lett.* **86**, 4167 (2001).
- ⁸ H. van Amerongen, L. Valkunas, and R. van Grondelle, *Photosynthetic Excitons* (World Scientific, Singapore, 2000).
- ⁹ B. Brüggemann and V. May, *J. Chem. Phys.* **118**, 746 (2003).
- ¹⁰ V. Sundström, T. Pullerits, and R. van Grondelle, *J. Phys. Chem. B* **103**, 2327 (1999).
- ¹¹ A. M. van Oijen, M. Ketelaars, J. Köhler, T. J. Aartsma, and J. Schmidt, *Science* **285**, 400 (1999).
- ¹² A. M. Van Oijen, M. Ketelaars, J. Köhler, T. J. Aartsma, and J. Schmidt, *Biophys. J.* **78**, 1570 (2000).
- ¹³ M. Matsushita, M. Ketelaars, A. M. van Oijen, J. Köhler, T. J. Aartsma, and J. Schmidt, *Biophys. J.* **80**, 1604 (2001).
- ¹⁴ M. A. Bopp, A. Sythnik, T. D. Howard, R. J. Cogdell, and R. M. Hochstrasser, *Proc. Natl. Acad. Sci. U.S.A.* **96**, 11271 (1999).
- ¹⁵ C. Tietz, C. O. Chekhlov, A. Dräbenstedt, J. Schuster, and J. Wrachtrup, *J. Phys. Chem. B* **103**, 6328 (1999).
- ¹⁶ C. Tietz, U. Gerken, F. Jelezko, and J. Wrachtrup, *J. Single Mol.* **1**, 67 (2000).
- ¹⁷ S. H. Lin, R. Alden, R. Islampour, H. Ma, and A. A. Villaeys, *Density Matrix Method and Femtosecond Processes* (World Scientific, Singapore, 1991).
- ¹⁸ S. Mukamel, *Principles of Nonlinear Optical Spectroscopy* (Oxford University Press, Oxford, 1995).
- ¹⁹ F. C. Spano and E. S. Manas, *J. Chem. Phys.* **103**, 5939 (1995).
- ²⁰ J. Knoester and F. C. Spano, in *J-Aggregates*, edited by T. Kobayashi (World Scientific, Singapore, 1996).
- ²¹ T. Meier, V. Chernyak, and S. Mukamel, *J. Phys. Chem. B* **101**, 7332 (1997).
- ²² O. Kühn and V. Sundström, *J. Chem. Phys.* **107**, 4154 (1997).
- ²³ L. D. Bakalis and J. Knoester, *J. Phys. Chem.* **103**, 6620 (1999).
- ²⁴ M. Dahlbom, T. Minami, V. Chernyak, T. Pullerits, V. Sundström, and S. Mukamel, *J. Phys. Chem. B* **104**, 3976 (2000).
- ²⁵ Th. Renger, V. May, and O. Kühn, *Phys. Rep.* **343**, 137 (2001).
- ²⁶ V. Novoderezhkin and R. van Grondelle, *J. Phys. Chem. B* **106**, 6025 (2002).
- ²⁷ B. Brüggemann, J. L. Herek, V. Sundström, T. Pullerits, and V. May, *J. Phys. Chem. B* **105**, 11391 (2001).
- ²⁸ V. May and Brüggemann, in *Femtochemistry and Femtobiology*, edited by A. Douhal and J. Santamaria (World Scientific, Singapore, 2002), p. 820.
- ²⁹ X. Hu, T. Ritz, A. Damjanovic, and K. Schulten, *J. Phys. Chem. B* **101**, 3854 (1997).
- ³⁰ M. G. Cory, M. C. Zerner, X. Hu, and K. Schulten, *J. Phys. Chem. B* **102**, 7640 (1998).
- ³¹ R. G. Alden, E. Johnson, V. Nagarajan, W. W. Parson, C. J. Law, and R. J. Cogdell, *J. Phys. Chem. B* **101**, 4667 (1997).

- ³²B. P. Krueger, G. D. Scholes, and G. R. Fleming, *J. Phys. Chem. B* **102**, 2284 (1998).
- ³³G. D. Scholes, I. R. Gould, R. J. Cogdell, and G. R. Fleming, *J. Phys. Chem. B* **103**, 2534 (1999).
- ³⁴V. May and O. Kühn, *Charge and Energy Transfer Dynamics in Molecular Systems* (Wiley-VCH, Weinheim, 1999).
- ³⁵O. Linden and V. May, *Eur. Phys. J. D* **12**, 473 (2000).
- ³⁶L. Seidner, G. Stock, and W. Domcke, *J. Chem. Phys.* **103**, 3998 (1995).
- ³⁷B. Wolfseder, L. Seidner, G. Stock, and W. Domcke, *Chem. Phys.* **217**, 275 (1997).
- ³⁸O. Kühn, V. Sundström, and T. Pullerits, *Chem. Phys.* **275**, 15 (2002).
- ³⁹M. Becker, V. Nagarajan, and W. W. Parson, *J. Am. Chem. Soc.* **113**, 6840 (1991).
- ⁴⁰A. Freiberg, J. A. Jackson, S. Lin, and N. W. Woodbory, *J. Phys. Chem. A* **102**, 4372 (1998).
- ⁴¹T. Polivka, T. Pullerits, J. L. Herek, and V. Sundström, *J. Phys. Chem. B* **104**, 1088 (2000).
- ⁴²K. Timpmann, Z. Katiliene, N. W. Woodbory, and A. Freiberg, *J. Phys. Chem. B* **105**, 12223 (2001).